

Solidification Simulation of Direct Energy Deposition Process by Multi-Phase Field Method Coupled with Thermal Analysis

Yusuke Shimono*†, Mototeru Oba*, and Sukeharu Nomoto*

* ITOCHU Techno-Solutions Corporation, 3-2-5, Kasumigaseki, Chiyoda-ku, Tokyo 100-6080 Japan

†Corresponding author

Email: yuusuke.shimono@ctc-g.co.jp

Abstract

The multi-phase field method coupled with the thermodynamics database of calculation of phase diagrams has been successfully applied to simulation of solidification microstructure evolutions in engineering casting processes. As multi-phase field method is based on the local (quasi-)equilibrium assumption in solidification theory [1], applying this method to solidification of additive manufacturing processes is not studied enough because of extremely large cooling rate and temperature gradient conditions. On the other hand, some researchers have reported experimental observations of the columnar-to-equiaxed transition in the solidification of the additive manufacturing processes including the direct energy deposition. They suggest that the local (quasi-)equilibrium assumption can be applied to solidification of additive manufacturing processes [2]. In this study, solidification microstructures of titanium alloys in direct energy deposition are calculated by multi-phase field method. Temperature distributions obtained by thermal analyses using finite element method are adapted to multi-phase field method. The microstructure evolution of columnar-to-equiaxed transition is confirmed. The results are summarized in a solidification map for direct energy deposition process conditions.

Introduction

Simulation methods according to the classical solidification theory based on the local equilibrium assumption enable prediction of the grain microstructure and morphological evolution. Among the models available for microstructure evolution, Monte Carlo simulations, cellular automata and the phase field method are the most widely used simulation methods [3]. The multi-phase field method (MPFM) coupled with the database of calculation of phase diagrams (CALPHAD) has been successfully applied for solidification microstructure evolution in standard casting condition.

In the classical solidification theory, the solidification map is also a useful tool for predicting solidification microstructure. The solidification map shows the columnar-to-equiaxed transition (CET) with functions of the temperature gradient G and growth rate R . Using the solidification map, we can predict the grain size and morphology of the solidification microstructure [4].

Additive manufacturing (AM) is currently used for a wide range of processes from low-cost consumer market to high-end direct metal systems. Direct energy deposition (DED) is a kind of AM method. It is often applied to produce large blank shapes. The cooling rate and temperature gradient in DED reach several thousand K/s and several hundred thousand K/m, respectively [5]. This process had been considered to be in non-equilibrium condition. The local equilibrium assumption of the classical solidification theory had been considered not to be applicable for the analysis of this process. On the other hand, some works have reported experimental observations of the CET in solidification of DED [6]. They suggest MPFM based on the local (quasi-)equilibrium assumption could possibly be adopted for the solidification simulation of DED process as well.

Many researchers consider the solidification map useful tool to predict solidification microstructure for AM process and have attempted to produce it by experiment [1, 6-8]. We attempt to investigate applicability of MPFM coupled with CALPHAD database for solidification simulation to DED process of a titanium alloy with

composition of Ti-6.5Al-3.5Mo-1.5Zr-0.3Si (wt.%). The solidification map is established with the microstructures obtained using various DED conditions.

Multi-Phase Field Method

The multi-phase field method proposed by Steinbach has been applied to many numerical simulation fields [1] and is expressed as shown below. The phase field parameter ϕ_i of a phase i in n multi-phases system is described by Equation (1).

$$\frac{\partial \phi_i}{\partial t} = \sum_{j=1}^n K_{ij} \left\{ \gamma_{ij} \left[\phi_j \nabla^2 \phi_j - \phi_i \nabla^2 \phi_i + \frac{\pi^2}{2\delta^2} (\phi_i - \phi_j) \right] + \frac{\pi}{\delta} \Delta G_{ij} \sqrt{\phi_i \phi_j} \right\} \quad (1)$$

K_{ij} is the interface mobility, γ_{ij} is the interface energy, δ is the interface thickness. ΔG_{ij} is the driving force for the transformation between the phases i and j . The driving force is obtained using the Gibbs free energy and chemical potential values estimated by CALPHAD database.

Overall composition c_α for N components system is dependent on the following diffusion equation:

$$\frac{dc_\alpha}{dt} = \nabla \cdot \sum_{i=1}^n \left[\phi_i \sum_{i=1}^{N-1} {}^i D_{\alpha\beta}^N \nabla c_\alpha^i \right] \quad (2)$$

Multi-phase diffusion for component α is then given as the sum of the flux in the individual phases, calculated from the composition gradients and the diagonal terms ${}^i D_{\alpha\beta}^N$ of the diffusivity matrix. The diffusivity matrix values are obtained by the CALPHAD database and diffusion mobility database.

In particular, CALPHAD database coupling method that uses the TQ-Interface of Thermo-Calc provides us opportunity to simulate the microstructure evolution of many engineering metal alloy processes [9]. For example, MICRESS® is a typical software tool for general commercial application of MPPM [10]. In this study, we used MICRESS for solidification simulation. We selected TCTI1 [11], which is the thermodynamic database for titanium based alloys including Ti, Al, Mo, Zr, Si, and MOBTI2 [12], which is the specialized titanium-based alloys diffusion mobility database.

Thermal Analysis of DED Process

The numerical simulations were performed according to the following steps:

- 1) Obtaining temperature profiles in a titanium alloy obstacle at different mass deposition rates.
- 2) Simulating solidification microstructure evolutions of the titanium alloy using MPPM for the temperature profiles obtained in step 1.
- 3) Establishment of the solidification map using results of step 2.

To execute thermal profile simulation for DED, we used a three-dimensional (3D) finite-element method (FEM) by thermal model implemented into ABAQUS [13], as shown in Figure 1. The element type was C3D8RT which was 8-node thermally coupled brick, trilinear displacement and temperature, reduced integration, hourglass control. The minimum mesh size was about 0.2mm.

We assumed that the thermal conductivity of substrate and deposited powder of the titanium alloy could be approximated as same as bulk metal one of Ti-6Al-4V [14]. The thermal conductivity values were referred by the Materials Properties Handbook [15] and ASM Handbook [16]. The initial uniform temperature of the metal region was set as 0 °C (273 K).

Figure 2 shows an image representing the thermal conduction simulation in this study.

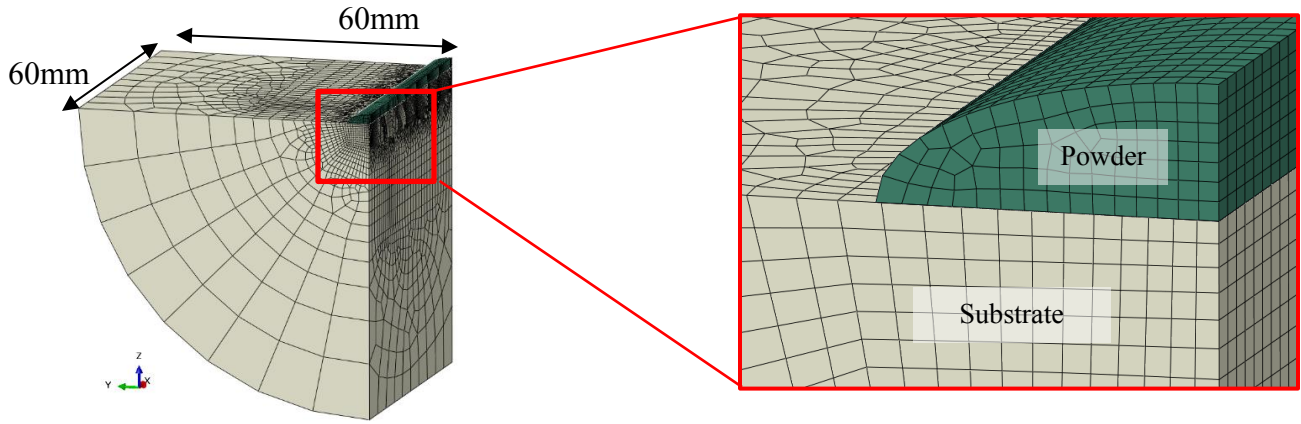


Figure 1. Finite element model for DED

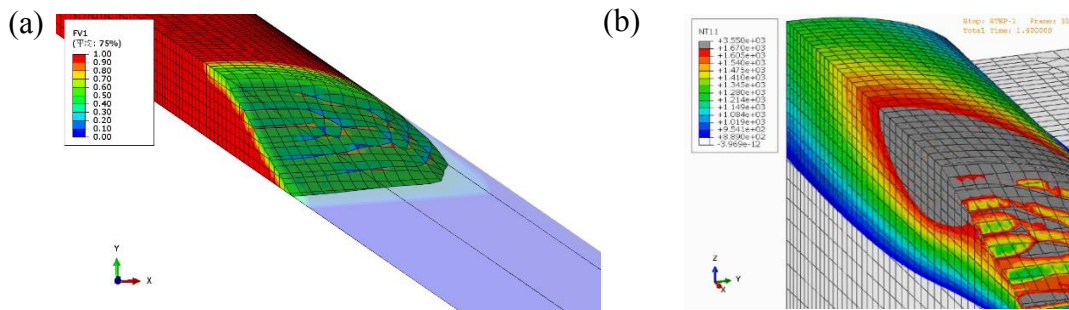


Figure 2. Snapshots of depositing (a) powder distribution, (b) temperature distribution

In DED processes, fluid flow of the melting pool is considered to be highly complex because of reciprocal effects between heat conduction, element diffusion, vaporization, convection and Marangoni convection [8, 17]. Therefore, it is still very difficult to perform solidification simulation accurately in three dimensions. In addition, it is necessary to predict the solidification microstructure transformation for various local temperature gradients and cooling rates for the establishment of solidification map. In this study, we simulated only the thermal conduction without taking the effect of fluid flow into account. We assumed that laser beam energy was entered only into the deposited powder. The powder distribution was defined as a Gaussian distribution. The laser power distribution was assumed to be uniform. Furthermore, in the solidification simulation, we selected a two-dimensional (2D) field on the plane perpendicular to beam scanning direction. This 2D solidification field was coupled with a one-dimensional (1D) temperature distribution parallel to the direction of the depth from the surface. The 1D temperature field was referred the three-dimensional (3D) temperature field at a time of the FEM thermal analysis. Figure 3 shows the procedure setting the 1D temperature field.

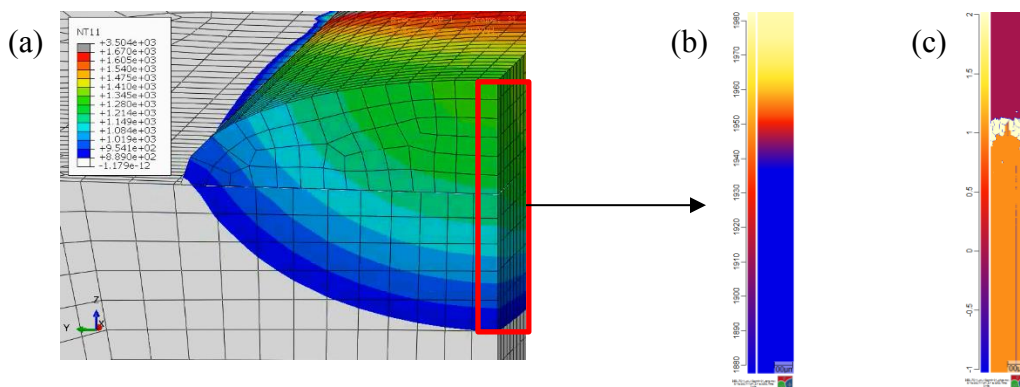


Figure 3. (a) A snapshot of temperature distribution of 3D FEM thermal simulation, (b) 1D temperature distribution obtained from (a), (c) Example of MPFM solidification simulation coupled with 1D temperature distribution in (b)

Calculation Conditions

In order to simulate CET varying with the temperature gradient and growth rate, we used nucleation conditions for equiaxed grains as shown in Table 1. The seed density model is a type of nucleation implemented in MICRESS [18]. This model is able to automatically select the density and radius of nuclei depending on undercooling of molten metal. Figure 4 shows the seed density distribution used in this study.

Table 1. Nucleation conditions of equiaxed grains

| Condition | Value |
|------------------------------------|-------------------------|
| Nucleation model | Seed density model [18] |
| Maximum nucleation temperature (K) | 1943 |
| Time interval (s) | 1×10^{-4} |
| Nucleation range | Liquid phase |
| Nuclei orientation | Random |

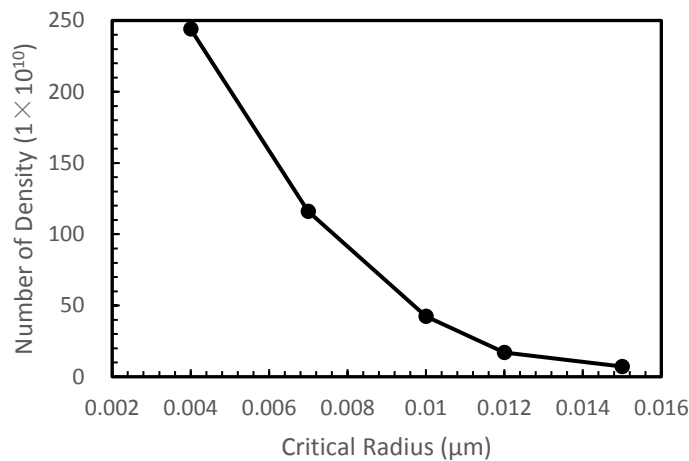


Figure 4. Seed density distribution in this study

The specification of laser beam is shown in Table 2. The deposition rates used in this study are shown in Table 3. We considered three cases with different deposition rates to obtain thermal profiles and solidification simulations using these thermal profiles. Melted zone and heat affected zone (HAZ) sizes were measured from the region where the temperature was over the melting temperature 1670 °C (1943 K) and the $\alpha\beta$ transformation temperature 889 °C (1162K), respectively. These temperatures were obtained using Thermo-Calc [19]. To compare results of simulation and to adjust parameters in FEM simulation, we referred to experiment data performed by Wang et.al. [2]. The sizes of deposited powder region are shown in Table 4 and Figure 5.

Table 2. Specification of laser beam

| | |
|-------------------------------|------|
| Laser Power (W) | 6000 |
| Beam Diameter (mm) | 6.0 |
| Beam Scanning Speed (mm/min.) | 1000 |

Table 3. Process conditions

| Case # | Deposition rate (g/min.) | Vertical length of melted zone (mm) | Vertical length of HAZ (mm) |
|--------|--------------------------|-------------------------------------|-----------------------------|
| 1 | 15.74 | 0.63 | 2.1 |
| 2 | 35.96 | 0.0 | 1.7 |
| 3 | 55.11 | 0.0 | 1.6 |

Table 4. Size of deposited powder region

| Case # | Height (mm) | Width (mm) |
|--------|-------------|------------|
| 1 | 0.58 | 3.9 |
| 2 | 1.36 | 3.8 |
| 3 | 1.76 | 4.5 |

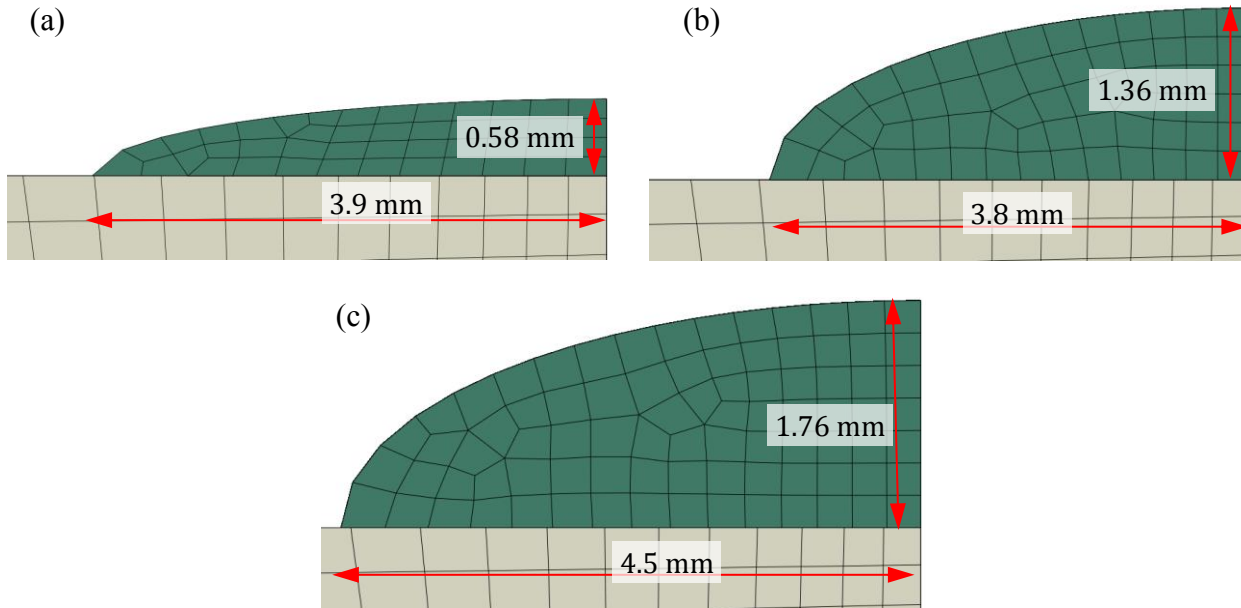
**Figure 5. Size of deposited powder region (a) Case 1, (b) Case 2, and (c) Case 3**

Table 5 shows the interface energy and interface mobility between liquid and β -Ti (BCC) in this study. The interface energy was estimated by the extended Becker's model [20, 21]. Table 6 shows geometry of simulation region for solidification with MPFM. Initial phase distributions were set liquid in the simulation region and columnar grains on the bottom boundary. Initial temperatures of liquid were set little higher than the melting point (1670 °C). This temperature was obtained using Thermo-Calc [19].

Table 5. Interface energy and interface mobility

| Interface energy (J/m ²) [19, 20] | Interface mobility (m ⁴ /Js) |
|---|---|
| 0.1 | 1.5×10^{-9} |

Table 6. Geometry of simulation region for solidification

| | |
|--------------------------------|--------------------------------------|
| Cell size | 1 $\mu\text{m} \times 1 \mu\text{m}$ |
| Number of cells | 50 \times 2000 |
| Width of solidification field | 50 μm |
| Height of solidification field | 2000 μm |

Results and Discussion

The phase distributions for MPFM solidification simulation and 1D temperature distribution obtained using FEM simulation for Cases 1, 2, and 3 are shown in Figure 6, 7, and 8, respectively. It can be seen that columnar grains grow from the melt pool bottom in all cases. After that, equiaxed grains nucleated in front of the growth direction of the columnar grains. Table 7 shows vertical lengths of equiaxed microstructure region from these results and experimental data [2].

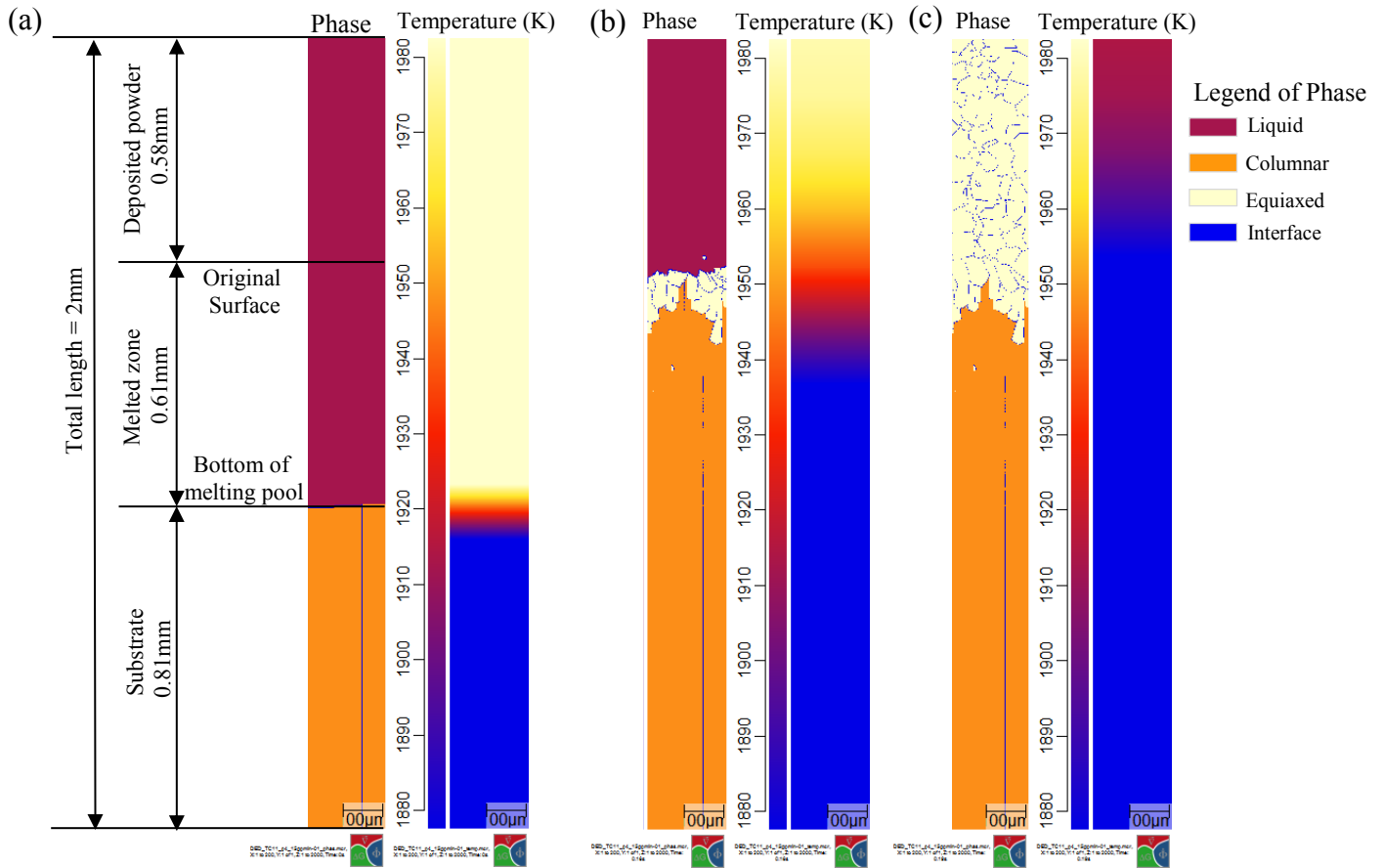


Figure 6. Phase and Temperature distributions of Case 1 (a) 0s, (b) 0.16s, and (c) 0.19s

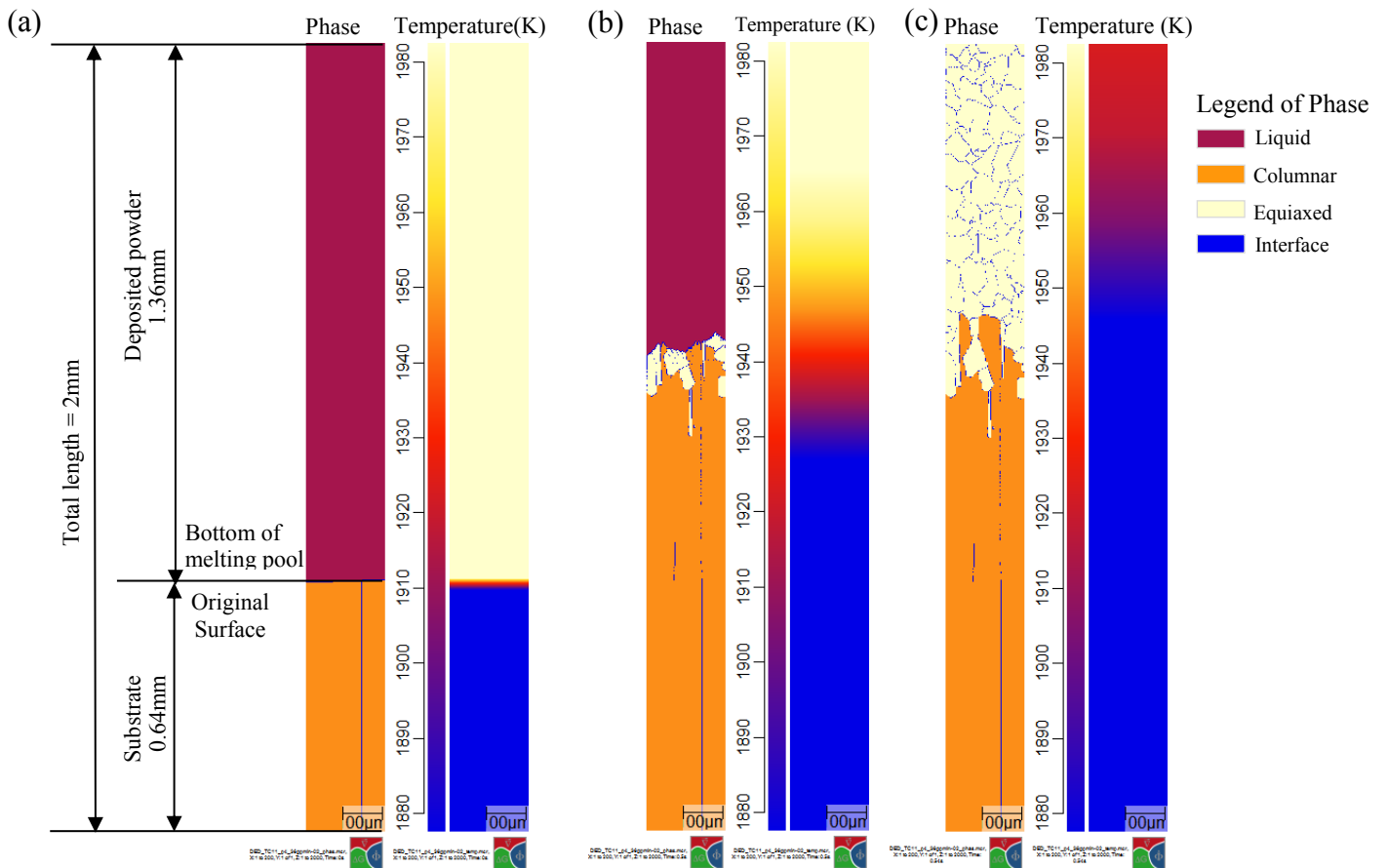


Figure 7. Phase and Temperature distributions of Case 2 (a) 0s, (b) 0.5s, and (c) 0.54

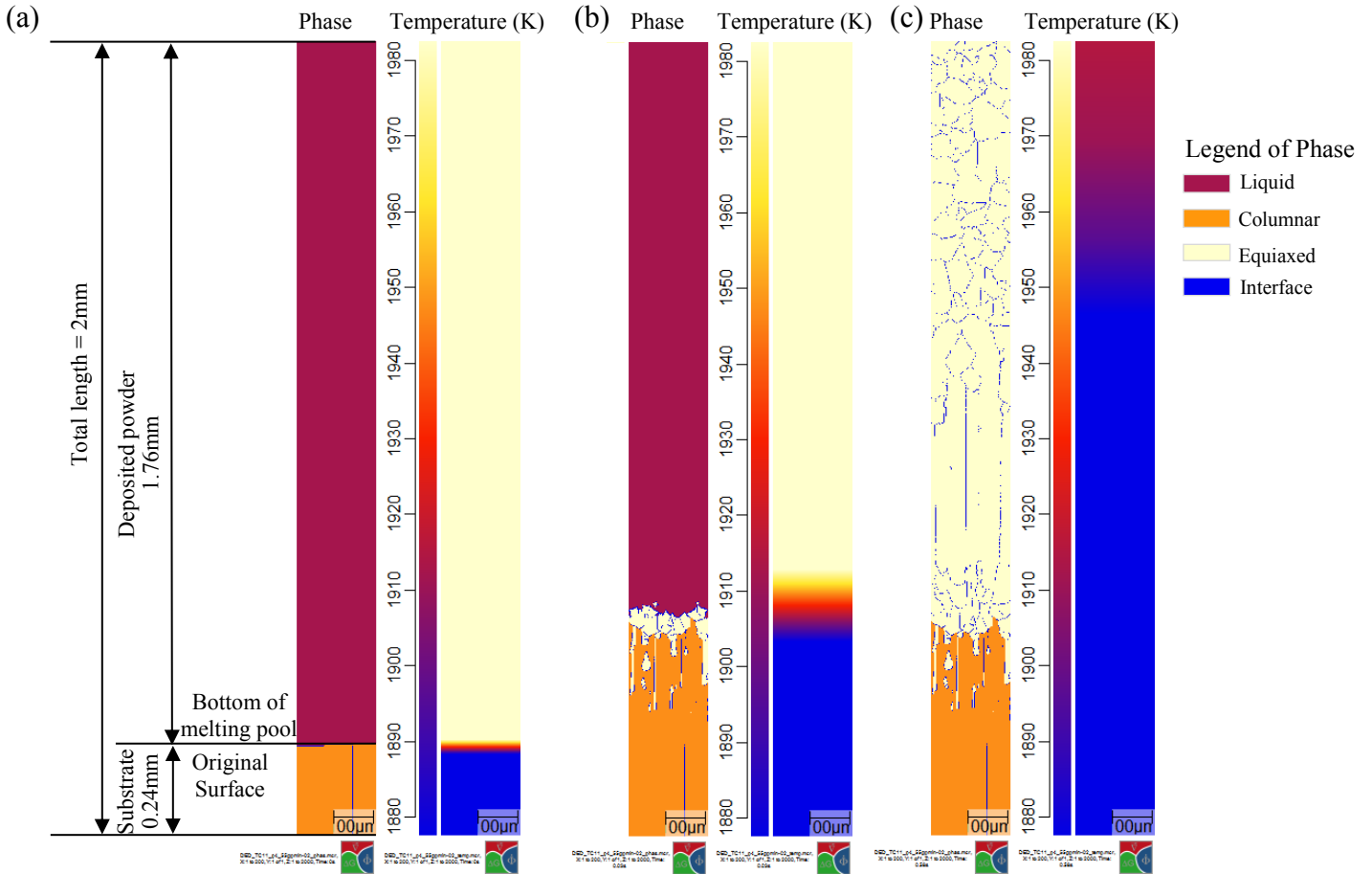


Figure 8. Phase and Temperature distributions of Case 3 (a) 0s, (b) 0.03s, and (c) 0.58

Table 7. Vertical length of equiaxed microstructure region

| Case # | Experiment (mm) | Simulation (mm) |
|--------|-----------------|-----------------|
| 1 | 0.7 | 0.8 |
| 2 | 1.1 | 1.0 |
| 3 | 1.6 | 1.7 |

Using the results of the solidification simulation with MPFM, temporal temperature gradient (G) and growth rate (R) on the liquid and solid interface for Cases 1, 2, and 3 are shown in Figure 9. The columnar, equiaxed and co-growth regions are indicated in Figure 9. The columnar growth points, the equiaxed growth points, and the co-growth points are plotted as circle, square, and triangle, respectively. It can be seen that there is co-growth region between the columnar and equiaxed regions. The black dashed lines show $G \times R$ which mean constant cooling rates. It can be seen that all points are nearly plotted along the constant cooling rate line ($G \times R = 1000\text{K/s}$). The columnar grains grow as dendrite from the melting pool bottom according to the constitutional undercooling due to the temperature gradient. After that, as the size of the melting pool becomes smaller, the temperature gradient becomes lower. The columnar-to-equiaxed transition happens due to higher undercooling. CET transient plots, co-growth plots, of three cases are located in the same area in Figure 9. It was confirmed reason why that the later cooling rate values closed each other even if the initial cooling rate values were different in these cases. In this way, the solidification microstructure based on the classical solidification theory is qualitatively confirmed in DED process.

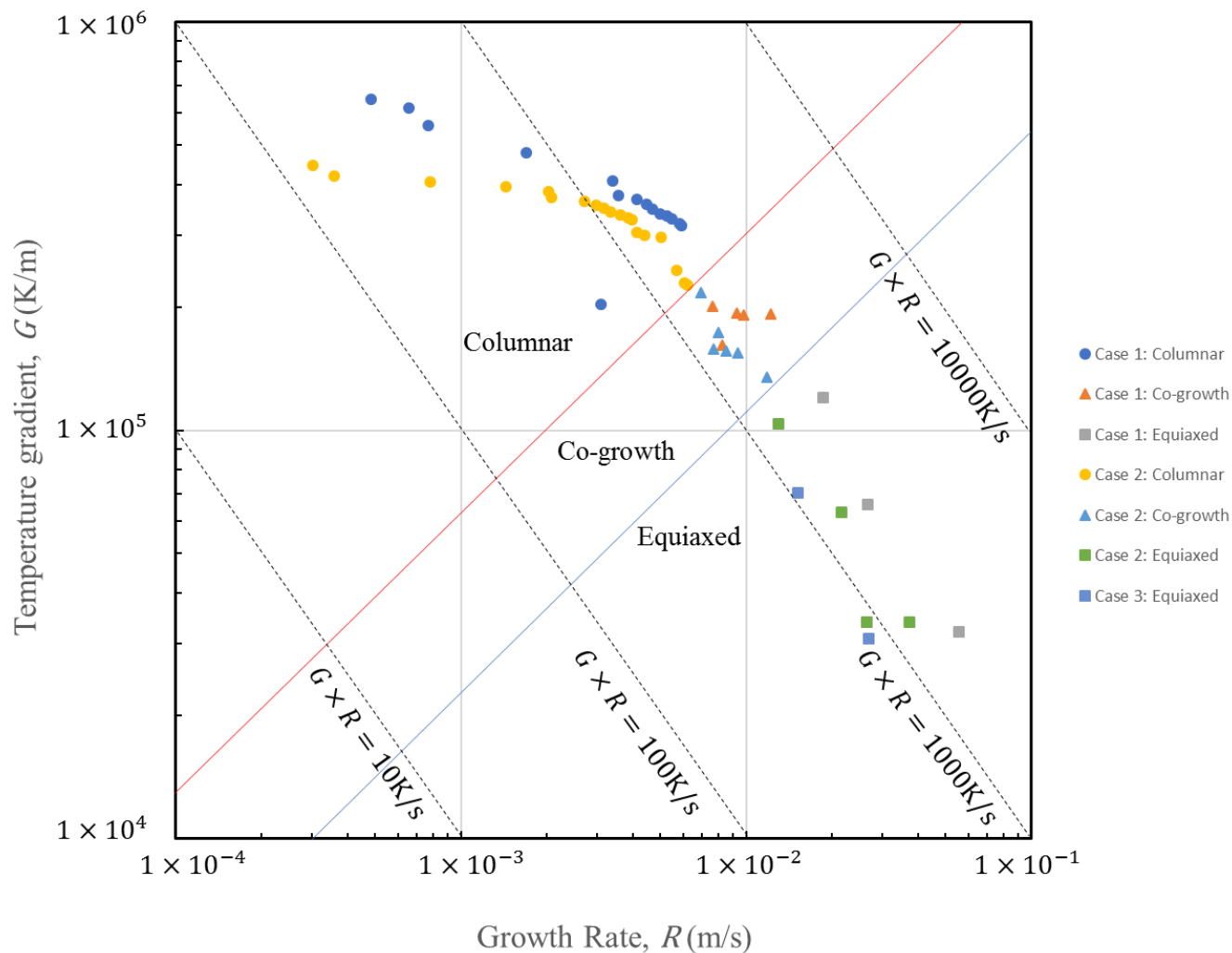


Figure 9. Solidification map of Ti-6.5Al-3.5Mo-1.5Zr-0.3Si in conditions of DED process model

Summary and Conclusion

We performed solidification simulation of Ti-6.5Al-3.5Mo-1.5Zr-0.3Si in DED process using MPFM coupled with CALPHAD database assuming local quasi-equilibrium. MPFM was also performed by coupling with a 1D temperature distribution obtained by FEM thermal conductivity analysis. We confirmed the CET simulation results for several DED conditions were qualitatively good agreement with experiment measurements. In addition, we indicated the possibility of constructing a solidification map for DED processes using the CET simulation results. It is confirmed that this numerical method offers significant potential for simulating the solidification microstructure evolution in DED processes.

References

- [1] J. Eiken, B. Boettger and I. Steinbach, "Multiphase-field approach for multicomponent alloys with extrapolation scheme for numerical application", *Phys. Rev. E*, 73 066122, 1-9, 2006.
- [2] T. Wang, Y.Y. Zhu, S.Q. Zhang, H.B. Tang, H.M. Wang, "Grain morphology evolution behavior of titanium alloy components during laser melting deposition additive manufacturing", *Journal of Alloys and Compounds*, 632, 505-513, 2015.
- [3] N. Xiao, Y. Chen, D. Li, and Y. Li, "Progress in mesoscopic modeling of microstructure evolution in steels" *Sci. China Technol. Sci.* 55, 341, 2012.

- [4] P. Kobryn and S. Semiatin, “Microstructure and Texture Evolution during Solidification Processing of Ti-6Al-4V”, *Journal of Materials Processing Technology*, 135, 330-339, 2003.
- [5] T. DebRoy, H.L. Wei, J.S. Zuback, T. Mukherjee, J.W. Elmer, J.O. Milewski, A.M. Beese, A. Wilson-Heid, A. De, W. Zhang, “Additive manufacturing of metallic components – Process, structure and properties”, *Progress in Materials Science*, 92, 112-224, 2018.
- [6] Y. M. Ren, X. Lin, X. Fu, H. Tan, J. Chen and W.D. Huang, “Microstructure and deformation behavior of Ti-6Al-4V alloy by high-power laser solid forming”, *Acta Materialia*, 132, 82-95, 2017.
- [7] S.S. Al-Bermani, M. L. Blackmore, W. Zhang and I. Todd, “The Origin of Microstructural Diversity, Texture, and Mechanical Properties in Electron Beam Melted Ti-6Al-4V”, *Metallurgical and materials transactions A*, 41A, 3422-3434, 2010.
- [8] P.C. Collins, D.A. Brice, P. Samini, I. Ghamarian, and H.L. Fraser, “Microstructural Control of Additively Manufactured Metallic Materials”, *Annu. Rev. Mater. Res.*, 46, 18.1-18.29, 2016.
- [9] Thermo-Calc Software AB, Software Development Kits:
<http://www.thermocalc.com/products-services/software/software-development-kits/>, 2018/6/28.
- [10] ACCESS e.V., MICRESS: <http://www.micress.de>, 2018/6/28.
- [11] Thermo-Calc Software AB, TCTI1 TCS Ti/TiAl-based Alloys Database, v1:
<http://www.thermocalc.com/products-services/databases/thermodynamic/>, 2018/6/28.
- [12] Thermo-Calc Software AB, MOBTI2 TCS Ti-alloys Mobility Database version, v2:
<http://www.thermocalc.com/products-services/databases/mobility/>, 2018/6/28.
- [13] Dassault Systèmes K.K., Abaqus Unified FEA
: <http://www.3ds.com/products-services/simulia/products/abaqus/>, 2016/3/24.
- [14] S. Bontha, N. W. Klingbeil, P. A. Kobryn, H. L. Fraser, “Effects of process variables and size-scale on solidification microstructure in beam-based fabrication of bulky 3D structures”, *Material Science and Engineering A*, 513-514, 311-318, 2009.
- [15] Materials Properties Handbook: Titanium Alloys, 1st ed., *ASM International*, 514-515, 1994.
- [16] ASM Handbook, Volume 15: Casting, *ASM International*, 468-481, 2008.
- [17] Y. Zhao, Y. Koizumi, K. Aoyagi, K. Yamanaka, and A. Chiba, “Modeling and Simulation of Electron Beam Additive Manufacturing for Biomedical Co-Cr-Mo Alloy”, *Proceedings of the Visual-JW2016*, 3, 48-49, 2016.
- [18] S. Nomoto, S. Minamoto and K. Nakajima, “Numerical Simulation for Grain Refinement of Aluminum Alloy by Multi-phase-field Model Coupled with CALPHAD”, *ISIJ International*, 49, 7, 1019–1023, 2009.
- [19] Thermo-Calc Software AB, Thermo-Calc: [http:// https://www.thermocalc.com/products-services/software/thermo-calc/](http://https://www.thermocalc.com/products-services/software/thermo-calc/), 2018/6/28
- [20] R. Becker, “Die Keimbildung bei der Ausscheidung in metallischen Mischkristallen”, *Ann. Phys.*, 424, 128–140, 1938.
- [21] Thermo-Calc Software AB, Precipitation module (TC-PRISMA): [http://www.thermocalc.com/products-services/software/precipitation-module-\(tc-prisma\)/](http://www.thermocalc.com/products-services/software/precipitation-module-(tc-prisma)/), 2018/6/28.